PCCP

PAPER

View Article Online
View Journal | View Issue

Cite this: *Phys. Chem. Chem. Phys.*, 2014, **16**, 8257

Solid state chemistry of nitrogen oxides – Part I: surface consumption of NO

M. Minissale,*[a] G. Fedoseev,[b] E. Congiu,[a] S. Ioppolo,[cd] F. Dulieu[a] and H. Linnartz[b]

Received 20th November 2013,
Accepted 14th March 2014

DOI: 10.1039/c3cp54917h

www.rsc.org/pccp

The role of nitrogen and oxygen chemistry in the interstellar medium is still rather poorly understood. Nitric oxide, NO, has been proposed as an important precursor in the formation of larger N- and O-bearing species, such as hydroxylamine, NH_2OH, and nitrogen oxides, NO_2 and N_2O. The topic of this study is the solid state consumption of NO *via* oxygenation and the formation of NO_2 and other nitrogen oxides ($ONNO_2$ and N_2O_4) under conditions close to those encountered on icy grains in quiescent interstellar clouds. In our experiments nitric oxide and oxygen allotropes (O, O_2, and O_3) or N atoms are co-deposited under ultra-high vacuum conditions on different substrates (silicate, graphite, compact ASW ice, and gold) at temperatures ranging between 10 and 35 K. Reaction products are monitored *via* Fourier Transform Reflection Absorption Infrared Spectroscopy (FT-RAIRS) and Temperature Programmed Desorption (TPD) using mass spectrometry. We find that NO_2 is efficiently formed in NO + $O/O_2/O_3$/N solid surface reactions. These are essentially barrier free and offer a pathway for the formation of NO_2 in space. Nitrogen dioxide, however, has not been astronomically detected, contradicting the efficient reaction channel found here. This is likely due to other pathways, including regular hydrogenation reactions, as discussed separately in part II of this study.

1 Introduction

Dark interstellar clouds act as birth sites of stars and planets, in which a complex network of sequential and parallel chemical processes, both in the gas phase and in the solid state, leads to the formation of larger molecules. Since gas-phase reactions alone cannot explain the full molecular complexity observed in space, it is generally accepted that more complex and saturated species form in the solid state through energetic (heating or hits by UV photons, X-rays, electrons or ions) and non-energetic (atom bombardment) processing.[1] Indeed, deep within dark clouds, temperatures drop as low as 10 K and with densities higher than 10^5 cm^{-3},[2] gas species accrete onto grains forming icy mantles. These regions are shielded from external UV light (other than local Ly-α emission from cosmic rays excited hydrogen) and the chemistry is largely driven by the impact of free atoms on icy dust. Atoms and unsaturated species diffuse in the ice, meet, and eventually react thermally or through tunneling[3–6] with the grain acting as a third body absorbing excess energy. Many of the bulk molecules observed in interstellar ice (*e.g.*, H_2O, CO_2, H_2CO, CH_3OH, HCOOH, CH_4, NH_3, and other nitrogen-bearing species[7–11]) form in this way. In later stages of the star formation process (*i.e.*, when the protostar has formed), the local UV field gains intensity and energetic processing becomes important, contributing also to molecular complexity in space.[12–14]

Over the past decade, a number of independent laboratory experiments have been performed to study surface reactions involving hydrogen, oxygen, carbon, and nitrogen atoms on cold surfaces.[15–22] The focus in these studies has been largely on hydrogen and oxygen chemistry, characterizing the solid state formation of water and methanol, for example. More recently a number of studies involving nitrogen have also been reported.[23] The solid state formation of NH_3 has been discussed[24] and NO ice was shown to be a good starting point in the formation of hydroxylamine, upon H-atom additions.[25–27] Both nitric oxide and ammonia are considered important precursor species in the formation of N-containing organics. NO, specifically, is a seed for N- and O-bearing species[28] such as NO_2, N_2O, HNO, HONO, HNO_3, and NH_2OH.

NO (^{14}N ^{16}O) was initially identified in the molecular clouds Sgr B2[29] and OMC1.[30] Nitric oxide has been identified in a number of different astrophysical regions, including star forming regions,[30] dark clouds,[31–33] hot cores,[34] PDRs,[35] and in the nucleus of the starburst galaxy NGC 253 – an extragalactic source.[36] NO can be

[a] *LERMA-LAMAp, Université de Cergy-Pontoise, Observatoire de Paris, ENS, UPMC, UMR 8112 du CNRS, 5 Mail Gay Lussac, 95000 Cergy Pontoise Cedex, France. E-mail: marco.minissale@obspm.fr*
[b] *Raymond and Beverly Sackler Laboratory for Astrophysics, Leiden Observatory, Leiden University, P.O. Box 9513, 2300 RA Leiden, The Netherlands*
[c] *Division of Geological and Planetary Sciences, California Institute of Technology, 1200 E. California Blvd., Pasadena, California 91125, USA*
[d] *Institute for Molecules and Materials, Radboud University Nijmegen, P.O. Box 9010, 6500 GL Nijmegen, The Netherlands*

easily formed and destroyed by two neutral–neutral gas-phase reactions:[37]

$$\bullet\ N + OH \rightarrow NO + H$$

$$\bullet\ NO + N \rightarrow N_2 + O.$$

Laboratory experiments have shown that NO is also formed through surface reactions, upon exposure of different ice mixtures (*i.e.*, H_2O:N_2, CO:N_2, and N_2:O_2) to different ions ($^{13}C^{2+}$, Ar^{2+}, N^+ and H^+, respectively) with energies in the range between 15–200 keV.[38–40] So far no evidence has been found that NO forms in non-energetic surface reactions like, for example, N + O. Astrochemical models predict typical NO abundances in the gas-phase, with respect to molecular hydrogen, of $f(NO/H_2) \approx 10^{-7}$–$10^{-6}$. The actual observed abundance[41] is about a factor 10 lower: $f(NO/H_2) \approx 10^{-8}$. This difference may be due to lacking destruction (*i.e.*, consumption) routes that have not taken correctly into account; actually large amounts of NO (up to 10% of the gas-phase abundance) are likely to accrete on the cold (10 K) dust grains, and therefore to react with H, O, and N atoms arriving from the gas-phase. It is not straightforward to estimate the relevance of solid NO as a starting point for the formation of more complex species. Reactions of NO with O-atoms have not been experimentally studied yet and this is the topic of the present study.

In this paper, part I in a two-article series, we present experimental results for NO + O, NO + O_2, NO + O_3, and NO + N reactions in the solid state that mainly lead to the formation of NO_2. Part II focusses on the surface consumption of NO_2 through NO_2 + H/O/N. This paper is organized as follows. The experimental setup and methods are described in the next section. Section 3 presents the experimental results. Section 4 discusses the possible reaction routes and physical chemistry of the N–O world. The findings are summarized in the conclusion.

2 Experimental

The experiments are performed using two different setups: FORMOLISM located in the LERMA-LAMAp laboratory at the University of Cergy-Pontoise (FR)[25] and SURFRESIDE[2] at the Sackler Laboratory for Astrophysics in Leiden (NL).[42] The possibility to perform similar experiments in two different setups allows us to study the same reaction pathways under different physical conditions, *i.e.*, different surface coverage (sub-monolayers – mainly FORMOLISM *vs.* multilayers – mainly SURFRESIDE[2]), different substrates (gold, silicates, graphite and amorphous solid water (ASW) ice), and different ice mixtures (pure NO, NO in polar ice, and NO in apolar ice).

Both setups comprise a central ultra-high vacuum chamber in which a sample holder is mounted in thermal contact with the cold finger of a closed-cycle He cryostat. The ice samples are studied *in situ* using Fourier Transform Reflection Absorption Infrared Spectroscopy (FT-RAIRS) and thermally relieved species are monitored in the gas phase by Temperature Programmed Desorption (TPD) using quadrupole mass spectrometry (QMS). Two different experimental procedures are applied. In pre-deposition experiments, ice is first deposited on the substrate and then exposed to the beam with reactants. This approach is necessary for O_3 as it is not possible to work with a pure ozone beam. Instead pure O_3 ice is obtained through annealing, causing other constituents than ozone to thermally desorb.[43,44,57,58] In pre-deposition experiments NO is subsequently deposited on top of the pure O_3 ice. In the case of O and O_2 experiments, all the reactants, including NO, are co-deposited. In all the experiments presented in this paper, unless otherwise specified, molecules of the most abundant isotopologues are used ($^{16}O_2$, $H_2{}^{16}O$, $^{14}N^{16}O$, and $^{14}N_2{}^{16}O$).

RAIR difference spectra are acquired during the exposure of the sample with respect to a background spectrum of the initial deposited ice at low temperature. In the case of co-deposition experiments, nitrogen oxide bearing ices are continuously deposited together with the reactant ices (NO + O and NO + O_2). In this case, RAIR difference spectra are acquired during co-deposition with respect to a background spectrum of the bare substrate at a low temperature. Once completed, the ice composition is further constrained using TPD, typically with rates of 1 up to 10 K min^{-1}.

As full descriptions of both setups are available in ref. 25 and 42 only the relevant details are given below.

2.1 FORMOLISM setup

The main chamber of the FORMOLISM setup[25,45] has a base pressure of 10^{-10}–10^{-11} mbar. It contains a non-porous amorphous olivine-type silicate (or a HOPG) sample surface (1 cm in diameter), operating at temperatures between 6.5 and 400 K. The silicate sample was obtained by thermal evaporation of San Carlos olivine ($Mg_{1.8}Fe_{0.2}SiO_4$) onto a gold-coated substrate (1 cm in diameter), operating at temperatures between 6.5 and 350 K. The density sites of adsorption are about the same as those of compact ice samples. Sample preparation and surface analysis are described extensively in Djouadi *et al.* (2005).[46] The temperature is controlled using a calibrated silicon-diode sensor and a thermocouple (AuFe/Chromel K-type) clamped to the sample holder. ASW ice can be grown *in situ* on the silicate sample. The H_2O vapour is obtained from deionized water previously purified by several freeze–pump–thaw cycles carried out under vacuum. H_2O molecules are deposited on the surface maintained at 110 K through a leak valve equipped with a microchannel doser positioned at 3.5 cm in front of the cold surface during the water ice deposition phase.

Two triply differentially pumped beam-lines are used to (co)deposit the reactants (NO and O, O_2, or O_3) onto the surface of the sample holder. Each beam line is equipped with a microwave dissociation source (a Surfatron cavity delivering 300 W at 2.45 GHz) that can generate oxygen atoms (in the ^3P ground state) from O_2. The O_2 dissociation efficiency is τ = 65–70%. The flux of O atoms arriving onto the surface is $\phi_O = 2\tau\phi O_2$, where ϕ_{O_2} = 3.2 ($\pm$0.3) $\times$ 10^{12} molecules cm^{-2} s^{-1} is the flux of O_2 molecules.[61] The flux of O atoms, consequently, is estimated to be 4.4($\pm$0.4) $\times$ 10^{12} atoms cm^{-2} s^{-1}. The (direct) flux of NO molecules at the surface is 2.8($\pm$0.2) $\times$ 10^{12} molecules cm^{-2} s^{-1}.

2.2 SURFRESIDE^2 setup

SURFRESIDE^2 comprises three distinct UHV chambers: a main chamber and two beam lines. Base pressures are better than 10^{-10} mbar. In the main chamber, ices can be deposited with monolayer precision on a gold substrate and processed at astronomically relevant temperatures. The substrate temperature is varied between 12 and 300 K with a relative precision of 0.5 K through a cryogenic temperature controller (LakeShore model 340). Ices are monitored *in situ* by means of RAIRS using a commercial FTIR, which covers the range between 4000 and 700 cm^{-1} (2.5–14 μm). TPD is used as a complementary analytical tool to constrain the experimental results. In the two beam lines different atom sources are used to produce atoms and radicals: (i) a thermal cracking source[47–49] is used to generate controlled beams of H/D atoms and (ii) a microwave discharge source[50,51] is used to generate O atoms that are co-deposited with NO-containing mixtures onto the substrate. This source has a 2.45 GHz microwave power supply (Sairem) that produces up to 300 W of power that is coupled into a microwave cavity, where atoms are generated in a plasma. All electronically and ro-vibrationally excited species generated in the plasma are energetically quenched through multiple collisions on passing through a quartz pipe before reaching the sample surface. Different plasma cavity pressures and/or different plasma power values give access to a tunable range of atom fluxes covering roughly 10^{11} and 10^{13} atoms cm^{-2} s^{-1}. In the present experiment, O and N atoms are obtained from N_2O and N_2 dissociation, respectively (see ref. 42). The effective O- and N-atom flux at the surface are $1(\pm0.3) \times 10^{11}$ and 9×10^{10} atoms cm^{-2} s^{-1}, respectively. Shutters separate the beam line chambers from the main chamber and allow for an independent operation of the individual beam lines.

In the following sections the experiments are not specifically labeled as FORMOLISM or SURFRESIDE^2 based, instead an overview of all experiments performed is given in Table 1.

3 Results

Fig. 1 shows four TPD curves of NO (mass 30, left-panel) and NO_2 (mass 46, right-panel) as obtained after completion of different experiments in the (sub)monolayer (ML) regime: 0.4 ML NO (black curve), 0.4 ML NO + 1.5 ML O (red curve), 0.4 ML NO + 1.5 ML O_2 (green curve), and 0.4 ML NO + 1.5 ML O_3 (blue curve) on a silicate sample held at 10 K. In our experiments, the desorption of NO takes place between 43 and 60 K, while NO_2 desorbs between 110 and 140 K. The left panel of Fig. 1 clearly shows that NO is consumed when oxygenated. In particular, when O atoms are co-deposited with NO molecules, they react and less than 10% of NO remains. This is about 40% in the case of O_3 molecules, while in the case of O_2 up to 70% of NO does not react. In parallel, the integrated area under the NO_2 TPD curves in Fig. 1 (right panel) anti-correlates with the corresponding integrated area of the NO TPD curve; a smaller amount of NO left on the cold surface after oxygenation corresponds to a larger amount of NO_2 formed in the ice.

In the next section we present RAIRS results, separately for NO + O, NO + O_2, NO + O_3, and NO + N.

3.1 NO + O

The NO + O reaction was studied by co-depositing reactants on different substrates (silicate and gold), and in different ice environments (pure NO + O, NO:H_2O + O, and NO:CO + O). In addition, as shown in Table 1, we performed every single experiment under different coverage conditions. The sub-monolayer regimes cover from 0.1 to 1 ML and the multilayer regimes are in the range of 1 to 10 ML.

As mentioned before, oxygen atoms are obtained *via* O_2 (FORMOLISM) or N_2O (SURFRESIDE^2) dissociation. In the first case, the O_2 dissociation is not complete (65%), and, therefore, some oxygen molecules may still reach the surface and react with NO. In the second case, undissociated N_2O molecules are still present, but the probability of forming O_2 molecules is very low (see ref. 42). An advantage of using N_2O is that it does not react with NO (and other nitrogen oxides) or O atoms.[42]

Fig. 2 shows four RAIR spectra recorded for a silicate sample held at 10 K using O_2 dissociation. Curve (a) shows the unprocessed spectrum for 1.5 ML of NO. Curves (b) and (c) show the results of a co-deposition resulting in 1.5 and 3.5 ML thick ice of NO + O + O_2 in a mixing ratio (3 : 3 : 1), respectively. Curve (d) shows the spectrum for deposition conditions used in curve (c), but after annealing to 86 K and cooling down to 50 K.

In curve (a) the NO (dimer) symmetric and asymmetric N–O stretch modes can be seen at around 1861 and 1770 cm^{-1}. The other three curves are clearly different with a number of new spectral features. Peaks at 1304–1311 and 1602 cm^{-1} are due to both NO_2 and $ONNO_2$ (*i.e.*, N_2O_3). Peaks at 1878, 1741 and 1256 cm^{-1} are due to N_2O_4. The peak at 1834 cm^{-1} is also due to $ONNO_2$ (N═O stretch). This latter peak does not show up in curve (d) indicating that $ONNO_2$ is not present at high temperature (>80 K). For this reason, in curve (d), we think that peaks at 1304–1311 and 1602 cm^{-1} are due to NO_2 ice. Here annealing offers an additional tool in assigning the bands. For instance, both NO dimer and N_2O_4 can contribute to the bands shown in curve (c) between 1890–1850 and 1755–1730 cm^{-1}. However, since the spectrum in curve d is obtained after annealing to 86 K – at this temperature all NO molecules have desorbed – the peaks at 1878 and 1741 cm^{-1} can only be due to N_2O_4. This facilitates the overall assignment of all spectra.

Fig. 3 shows four more RAIR spectra (with two zoom-ins), now explicitly involving water in the 15 K deposition process simulating a polar environment. In curve (a) the resulting spectrum of a co-deposition of the dissociation products from an N_2O plasma with H_2O (O : N_2O : H_2O = 1 : 10 : 500) is shown. In curves (b) and (c) the co-deposition spectra have extra features due to added NO; mixing ratios of O : NO : N_2O : H_2O = 1 : 2 : 10 : 500 and 1 : 10 : 10 : 500 are applied, respectively. Curve (d) shows the spectrum resulting from co-deposition of N_2O dissociation products with H_2O and $^{18}O_2$ molecules (O : $^{18}O_2$: N_2O : H_2O = 1 : 10 : 10 : 500).

In this case the oxygen atoms originate from N_2O dissociation, and the resulting RAIR spectra are very similar to those

Table 1 List of experiments

SURFRESIDE[2]

Experiment	Method	Ratio	R_{dep} (L min^{-1}) NO, ^{13}CO	T_{dep} (K)	$T_{atom\text{-}add}$ (K)	P_{AL} (10^{-6} mbar)	MWP (W)	Atom-fluence (10^{16} atoms per cm^2)	t (min)	RAIRS	TPD
O + N_2O + ^{13}CO	co-dep	1 : 10 : 500	—, 4	15	15	2	275	0.01	15	Y	—
O + NO + N_2O + ^{13}CO	co-dep	1 : 2 : 10 : 500	0.015, 4	15	15	2	275	0.01	15	Y	—
O + NO + N_2O + ^{13}CO	co-dep	1 : 10 : 10 : 500	0.08, 4	15	15	2	275	0.01	15	Y	—

Experiment	Method	Ratio	R_{dep} (L min^{-1}) NO, H_2O	T_{dep} (K)	$T_{atom\text{-}add}$ (K)	P_{AL} (10^{-6} mbar)	MWP (W)	Atom-fluence (10^{16} atoms per cm^2)	t (min)	RAIRS	TPD
O + N_2O + H_2O	co-dep	1 : 10 : 500	—, 4	15	15	2	275	0.01	15	Y	—
O + NO + N_2O + H_2O	co-dep	1 : 2 : 10 : 500	0.015, 4	15	15	2	275	0.01	15	Y	—
O + NO + N_2O + H_2O	co-dep	1 : 10 : 10 : 500	0.08, 4	15	15	2	275	0.01	15	Y	—

Experiment	Method	Ratio	R_{dep} (L min^{-1}) $^{18}O_2$, ^{13}CO	T_{dep} (K)	$T_{atom\text{-}add}$ (K)	P_{AL} (10^{-6} mbar)	MWP (W)	Atom-fluence (10^{16} atoms per cm^2)	t (min)	RAIRS	TPD
O + $^{18}O_2$ + N_2O + ^{13}CO	co-dep	1 : 10 : 10 : 500	0.08, 4	15	15	2	275	0.01	15	Y	—
O + $^{18}O_2$ + N_2O + ^{13}CO	co-dep	1 : 50 : 10 : 500	0.4, 4	15	15	2	275	0.02	30	Y	—

Experiment	Method	Ratio	R_{dep} (L min^{-1}) $^{18}O_2$, H_2O	T_{dep} (K)	$T_{atom\text{-}add}$ (K)	P_{AL} (10^{-6} mbar)	MWP (W)	Atom-fluence (10^{16} atoms per cm^2)	t (min)	RAIRS	TPD
O + $^{18}O_2$ + N_2O + H_2O	co-dep	1 : 50 : 10 : 500	0.4, 4	15	15	2	275	0.02	30	Y	—

Experiment	Method	Ratio	R_{dep} (L min^{-1}) NO	T_{dep} (K)	$T_{atom\text{-}add}$ (K)	P_{AL} (10^{-6} mbar)	MWP (W)	Atom-fluence (10^{16} atoms per cm^2)	t (min)	RAIRS	TPD
^{15}N + $^{15}N_2$	co-dep	1 : 100	—	15	15	8	300	0.03	60	Y	—
$^{15}N_2$ + NO	co-dep	1 : 5	2.5	15	15	8	300	—	90	Y	—
^{15}N + $^{15}N_2$ + NO	co-dep	1 : 100 : 500	2.5	15	15	8	300	0.045	90	Y	—

Table 1 (*continued*)

FORMOLISM

Experiment	Method	Thickness (ML)	R_{dep} (L min^{-1}) NO, O_2 on $(SiO)_2$	T_{dep} (K)	$T_{atom\text{-}add}$ (K)	P_{AL} (10^{-10} mbar)	MWP (W)	Atom-fluence (10^{16} atoms per cm^2) (O from O_2)	t (min)	RAIRS	TPD
NO + O + O_2	co-dep	0.5	0.09, 0.025	15	15	1.9	90	0.17	6	N	QMS
NO + O + O_2	co-dep	0.5	0.09, 0.025	25	25	1.9	90	0.17	6	N	QMS
NO + O + O_2	co-dep	0.5	0.09, 0.025	35	35	1.9	90	0.17	6	N	QMS
NO + O + O_2	co-dep	1.2	0.09, 0.025	10	10	1.9	90	0.2	8	Y	QMS

Experiment	Method	Thickness (ML)	R_{dep} (L min^{-1}) NO, O_2 on graphite	T_{dep} (K)	$T_{atom\text{-}add}$ (K)	P_{AL} (10^{-10} mbar)	MWP (W)	Atom-fluence (10^{16} atoms per cm^2)	t (min)	RAIRS	TPD
NO + O + O_2	co-dep	0.5	0.12, 0.035	10	10	1.9	90	0.17	6	N	QMS
NO + O + O_2	co-dep	0.5	0.12, 0.035	10	10	1.9	90	0.17	6	N	QMS

Experiment	Method	Thickness (ML)	R_{dep} (L min^{-1}) H_2O, NO, O_2	T_{dep} (K)	$T_{atom\text{-}add}$ (K)	P_{AL} (10^{-10} mbar)	MWP (W)	Atom-fluence (10^{16} atoms per cm^2)	t (min)	RAIRS	TPD
H_2O + NO + O + O_2	co-dep	50 : 0.3	2.4, 0.08, 0.02	10	10	1.9	80	0.05	2	N	QMS
H_2O + NO + O + O_2	seq-dep	50 : 0.3	2.4, 0.08, 0.02	10	10	1.9	80	0.2	8	N	QMS
H_2O + NO + O + O_2	seq-dep	50 : 1.1	2.4, 0.08, 0.02	10	10	1.9	80	0.7	24	N	QMS
H_2O + NO + O + O_2	co-dep	50 : 5	2.4, 0.08, 0.02	10	10	1.9	90	1	35	Y	QMS

Experiment	Method	Thickness (ML)	R_{dep} (L min^{-1}) O_2, NO[a] on $(SiO)_2$	T_{dep} (K)	$T_{atom\text{-}add}$ (K)	P_{AL} (10^{-10} mbar)	MWP (W)	Atom-fluence (10^{16} atoms per cm^2)	t (min)	RAIRS	TPD
NO + O_2	co-dep	0.5 : 1	0.08, 0.09	10	10	—	—	—	—	N	QMS
NO + O_2	seq-dep	0.5 : 1	0.08, 0.09	10	10	—	—	—	—	N	QMS
O_2 + NO	seq-dep	0.5 : 1	0.08, 0.09	10	10	—	—	—	—	N	QMS
NO + O_2	co-dep	2.5 : 5	0.08, 0.09	10	10	—	—	—	—	Y	QMS

Experiment	Method	Thickness (ML)	R_{dep} (L min^{-1}) O_2, NO[a] on graphite	T_{dep} (K)	$T_{atom\text{-}add}$ (K)	P_{AL} (10^{-10} mbar)	MWP (W)	Atom-fluence (10^{16} atoms per cm^2)	t (min)	RAIRS	TPD
NO + O_2	co-dep	1 : 1	0.09, 0.1	10	10	—	—	—	—	N	QMS
NO + O_2	seq-dep	1 : 1	0.09, 0.1	10	10	—	—	—	—	N	QMS

Experiment	Method	Thickness (ML)	R_{dep} (L min^{-1}) H_2O, O_2, NO[a]	T_{dep} (K)	$T_{atom\text{-}add}$ (K)	P_{AL} (10^{-10} mbar)	MWP (W)	Atom-fluence (10^{16} atoms per cm^2)	t (min)	RAIRS	TPD
H_2O + NO + O_2	co-dep	50 : 0.5 : 1	2.4, 0.08, 0.09	10	10	—	—	—	—	N	QMS
H_2O + NO + O_2	seq-dep	50 : 1 : 1	2.4, 0.08, 0.09	10	10	—	—	—	—	N	QMS
H_2O + O_2 + NO	seq-dep	50 : 1 : 2	2.4, 0.08, 0.09	10	10	—	—	—	—	Y	QMS
H_2O + NO + O + O_2	co-dep	50 : 2 : 4	2.4, 0.08, 0.09	10	10	—	—	—	—	Y	QMS

Experiment	Method	Thickness (ML)	R_{dep} (L min^{-1}) O_3, NO on $(SiO)_2$	T_{dep} (K)	$T_{atom\text{-}add}$ (K)	P_{AL} (10^{-10} mbar)	MWP (W)	Atom-fluence (10^{16} atoms per cm^2)	t (min)	RAIRS	TPD
O_3 + NO	seq-dep	1.2 : 0.2	0.09, 0.1	10	10	—	—	—	—	N	QMS
O_3 + NO	seq-dep	1.2 : 0.4	0.09, 0.1	10	10	—	—	—	—	N	QMS
O_3 + NO	seq-dep	1.2 : 0.6	0.09, 0.1	10	10	—	—	—	—	N	QMS
O_3 + NO	seq-dep	1.2 : 0.8	0.09, 0.1	10	10	—	—	—	—	N	QMS
O_3 + NO	seq-dep	1.2 : 1.4	0.09, 0.1	10	10	—	—	—	—	N	QMS

Table 1 (*continued*)

FORMOLISM											
			R_{dep} (L min^{-1})								
Experiment	Method	Thickness (ML)	O_3, NO on $(SiO)_2$	T_{dep} (K)	$T_{atom\text{-}add}$ (K)	P_{AL} (10^{-10} mbar)	MWP (W)	Atom-fluence (10^{16} atoms per cm^2)	t (min)	RAIRS	TPD
O_3 + NO	seq-dep	1.2 : 2	0.09, 0.1	10	10	—	—	—	—	N	QMS
O_3 + NO	seq-dep	1.5 : 0.2	0.09, 0.1	10	10	—	—	—	—	Y	QMS
O_3 + NO	seq-dep	1.5 : 0.4	0.09, 0.1	10	10	—	—	—	—	Y	QMS
O_3 + NO	seq-dep	1.5 : 0.6	0.09, 0.1	10	10	—	—	—	—	Y	QMS
O_3 + NO	seq-dep	1.5 : 0.9	0.09, 0.1	10	10	—	—	—	—	Y	QMS
O_3 + NO	seq-dep	1.5 : 1.8	0.09, 0.1	10	10	—	—	—	—	Y	QMS
O_3 + NO	seq-dep	1.5 : 3.5	0.09, 0.1	10	10	—	—	—	—	Y	QMS
			R_{dep} (L min^{-1})								
Experiment	Method	Thickness (ML)	H_2O, O_3, NO	T_{dep} (K)	$T_{atom\text{-}add}$ (K)	P_{AL} (10^{-10} mbar)	MWP (W)	Atom-fluence (10^{16} atoms per cm^2)	t (min)	RAIRS	TPD
H_2O + O_3 + NO	seq-dep	50 : 1.2 : 1.2	2.4, 0.08, 0.09	10	10	—	—	—	—	Y	QMS

Sequential deposition (seq-dep), co-deposition (co-dep), and deposition of single species (dep) are performed under different laboratory conditions. The thickness is expressed in monolayers (ML); R_{dep} is the deposition rate of a selected molecule expressed in Langmuir (L) min^{-1}, where 1 L = 1.3×10^{-6} mbar s^{-1}; T_{dep} is the substrate temperature during deposition; $T_{atom\text{-}add}$ is the substrate temperature during atom addition; P_{AL} is the atomic line pressure during atom exposure; atom-fluence is the total fluence at the end of the experiment; t is the time of atom addition; RAIRS is the acquisition of RAIR spectra during seq-dep, co-dep, or dep of selected species; TPD is the temperature programmed desorption experiment performed afterward. [a] Minissale *et al.* (2013).[6]

Fig. 1 TPD curves of NO (mass 30, left-panel) and NO_2 (mass 46, right-panel) for four different (co)deposition experiments on silicate held at 10 K: 0.4 ML of NO (black line), 0.4 ML NO + 1.5 ML of O (red line), 0.4 ML NO + 1.5 ML of O_2 (green line) and 0.4 ML NO + 1.5 ML of O_3 (blue line).

Fig. 2 RAIR spectra obtained after deposition on a silicate sample held at 10 K of: (a) 1.5 ML of NO; (b) co-deposition of 1.5 ML NO + O; (c) co-deposition of 3.5 ML of NO + O; and (d) co-deposition of 3.5 ML of NO + O, annealing to 86 K and cooling down to 50 K.

shown in Fig. 2. Moreover, N_2O (see Table 2) and H_2O precursor features show up in the spectra. The latter in particular does not allow an unambiguous identification of solid NO_2 in curves (b) through (d). The two insets of Fig. 3 show bands due to NO dimer, NO_2 and $ONNO_2$ that only show up when NO is co-deposited with O-atoms. Furthermore, curve (c) shows peaks of NO and N_2O that are also present in the other curves, including the peak in curve (a) at 1861 cm^{-1} due to *cis*-$(NO)_2$ and two more peaks due to $ONNO_2$ at 1834 and 1304 cm^{-1}. The presence of *cis*-$(NO)_2$ in the ice can be explained by a high NO concentration, while the other two features arise from surface reactions, as will be discussed later. With respect to the previous experiments performed on the silicate sample, here all peak positions are somewhat shifted (5 cm^{-1} at maximum) because of the polar environment the species are embedded in.

Finally, we have studied the NO + O reaction in a ^{13}CO matrix, *i.e.*, an apolar environment. Fig. 4 shows four more RAIR co-deposition spectra at 15 K. Curve (a) shows N_2O dissociation products with ^{13}CO molecules ($O : N_2O : {}^{13}CO$ = 1 : 10 : 500), curves (b) and (c) show N_2O dissociation products with ^{13}CO and NO molecules ($O : NO : N_2O : {}^{13}CO$ = 1 : 2 : 10 : 500 and 1 : 10 : 10 : 500, respectively), and curve (d) shows N_2O dissociation products with ^{13}CO and $^{18}O_2$ molecules ($O : {}^{18}O_2 : N_2O : {}^{13}CO$ = 1 : 50 : 10 : 500).

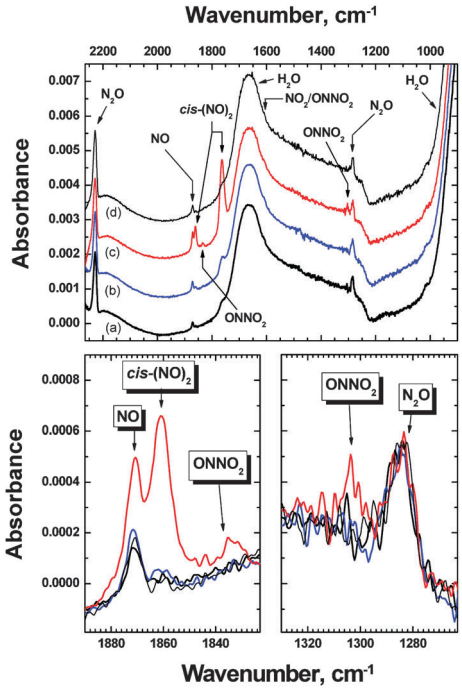

Fig. 3 Top panel: four RAIR spectra of co-depositions at 15 K of (a) N_2O plasma dissociation products with H_2O molecules; (b) and (c) N_2O plasma dissociation products with H_2O and NO molecules (two different mixing ratios, see text); and (d) N_2O plasma dissociation products with H_2O and $^{18}O_2$ molecules. The bottom panels show absorption features of solid $ONNO_2$ (N_2O_3) in two spectral regions.

In Fig. 4 the CO signatures (see Table 2) for different isotopologues (^{13}CO, ^{12}CO, $^{13}C^{17}O$ and $^{13}C^{18}O$), due to impurities present in the ^{13}CO bottle, are clearly visible. In this case, the region of the water bending mode is flat and allows a clear identification of NO_2 at 1614 cm^{-1}. The N_2O and NO (monomer) spectra are visible in each spectrum. While the N_2O band positions are almost the same in each spectrum, the band intensities actually depend on the mixing ratio of the deposited species. The NO band is also present in curve (a) although it is not deposited directly in the sample; actually it comes from the N_2O dissociation as evident in the left-hand panel of Fig. 4. The NO_2 monomer peak (at 1614 cm^{-1}) shows the same behaviour as the NO band. It is present in curves (a) and (b), but it gains absorption strength when NO molecules are deposited as shown in curves (b) and (c) (see the central panel of Fig. 4). O_3 is formed only when $^{18}O_2$ is co-deposited with NO and N_2O dissociation products (see curve d and the right-hand panel).

3.1.1 Dependence on substrate, coverage and temperature. The different substrates (silicate, compact ASW ice, and gold) and the ice composition used do not visibly affect the final products. They are, however, responsible for small shifts of the IR features. Surface coverage only slightly changes the final products of our experiments. In particular, multilayer regimes facilitate dimerization reactions, as we will discuss below in Section 4. In order to investigate any temperature dependence of the NO + O reaction, experiments are performed in which the deposition temperature was varied. Fig. 5 shows three NO TPD curves after deposition of 0.5 ML NO + 1 ML O on a silicate sample held at 15 K (dashed curve), 25 K (solid curve), and 35 K (dotted curve), respectively. The amount of NO left as a function of substrate temperature (calculated by integrating the area of each NO peak) is plotted in the inset of Fig. 5. Within the experimental error bars, this does not show any substantial temperature dependence. The reaction is already efficient at low temperatures and seems to be essentially barrier free.

Table 2 List of detected features in the RAIR spectra shown in Fig. 2–4, 6 and 7

		Substrate					
		$(SiO)_x$			H_2O ice	CO ice	Gold
		Experiment					
Molecule	Mode	NO + O	NO + O_2 (ref. 6) (cm^{-1})	NO + O_3	NO + N_2O* (cm^{-1})	NO + N_2O* (cm^{-1})	NO + N (cm^{-1})
NO		—	1897	—	1871	1876	—
cis-$(NO)_2$	N–O s-str ($a_g(1)$)	1861	1863	1874	1861	1865	1865
	N–O a-str ($b_u(5)$)	1770	1776	1773	1763	1770	1771
NO_2	N–O a-str	1602	1605	1612	1606	1614	1606
	N–O s-str	1304–1311	1311	1307	1304	1304	1307
$ONNO_2$	N═O str	1834	1834	1838	1835	1840	1836
	N–O a-str	1602	1605	1612	1606	1614	1606
	N–O s-str	1304–1311	1311	1307	1304	1304	1307
	NO_2 deform	—	—	—	—	—	774
N_2O_4	N═O str	1878	1875	1874	—	—	
	NO_2 a-str ($b_{3u}(11)$)	1741	—	—	—	—	
	NO_2 s-str ($b_{2u}(11)$)	1256	—	1255	—	—	
N_2O	NN str	—	—	—	2254	2240	2245
	N═O str	—	—	—	1284	1288	
$^{161616}O_3$	O–O a-str	—	—	1043	—	—	—
$^{181816}O_3$	O–O a-str	—	—	—	—	974	—
$^{12}C^{16}O$	C–O a-str	—	—	—	—	2094	—
$^{13}C^{16}O$	C–O a-str	—	—	—	—	2140	—
$^{13}C^{17}O$	C–O a-str	—	—	—	—	2020	—
$^{13}C^{18}O$	C–O a-str	—	—	—	—	1987	—

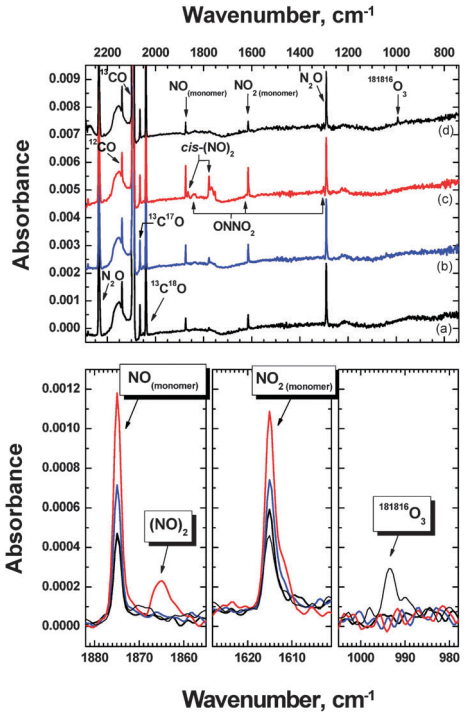

Fig. 4 Top panel: four RAIR co-deposition spectra at 15 K of: (a) N_2O plasma dissociation products with ^{13}CO molecules; (b) and (c) N_2O plasma dissociation products with ^{13}CO and NO molecules (two different mixing ratios, see text); and (d) N_2O plasma dissociation products with ^{13}CO and $^{18}O_2$ molecules. The zoom-in panels show absorption features of NO, NO_2, and O_3 in three different spectral regions.

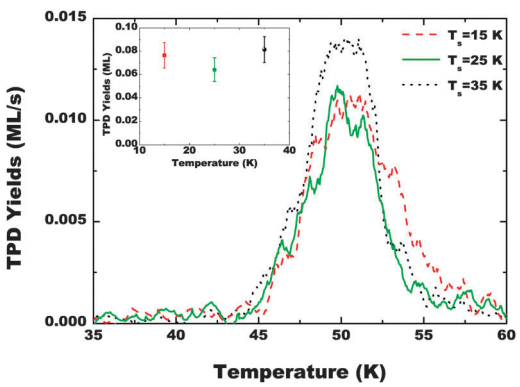

Fig. 5 Three TPD (mass 30) plots of NO after deposition of 0.5 ML NO + 1 ML O at different temperatures: 15 K (dashed), 25 K (solid) and 35 K (dotted). The inset shows the integrated area under the TPD curves.

3.2 NO + O_2

This reaction has been studied in detail before,[6] and is discussed here merely for completeness, as this reaction channel is intimately linked to the other two reactions presented here – NO + O and NO + O_3.

In the NO + O experiments the reaction NO + O_2 can take place for two reasons: (i) the oxygen plasma (generated from cracking O_2 molecules) is not fully atomic, and about 20–30% of O_2 molecules remain; and (ii) O_2 molecules can also form on the cold surface due to O + O recombinations. In the NO + O_3 experiments, O_2 molecules are formed through the reaction itself. In Fig. 6 a RAIR spectrum of 5 ML O_2 + 2.5 ML NO co-deposited at 10 K on a silicate surface is shown (taken from ref. 6). The features at 1897 and 1902 cm^{-1} are assigned to the NO monomer,[52] and bands at 1863 and 1776 cm^{-1} are signatures of the NO dimer.[52] N_2O_4 is represented by a band at 1875 cm^{-1}.[53] The broad band at 1311 cm^{-1} is attributed to the ν(N–O) symmetric stretch and the band at 1605 cm^{-1} to the ν(N–O) asymmetric stretch of NO_2.[54,55] The band at 1832 cm^{-1} originates from the asymmetric stretch of $ONNO_2$[56] that most likely also contributes to the bands at 1311 cm^{-1} and 1605 cm^{-1}. These data are summarized in Table 2.

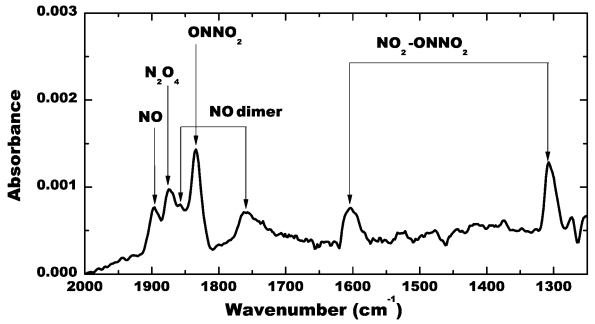

Fig. 6 Adapted from Minissale *et al.* (2013).[6] RAIR spectrum of 5 ML O_2 + 2.5 ML NO co-deposited at 10 K on a silicate surface. Seven features due to NO, $(NO)_2$, NO_2, $ONNO_2$ and N_2O_4 are labelled.

As described in ref. 6 this illustrates that in NO + O_2 solid state interactions nitrogen dioxide is formed.

3.3 NO + O_3

In Fig. 7 the results are presented for 1.5 ML pre-deposited O_3 being exposed to increasing doses of NO at 10 K. In this specific case the species are not co-deposited on the surface, as in the case of NO + O and NO + O_2, but O_3 is first deposited and subsequently bombarded with NO. This procedure does not permit to work with high coverages (more than 2 ML) because

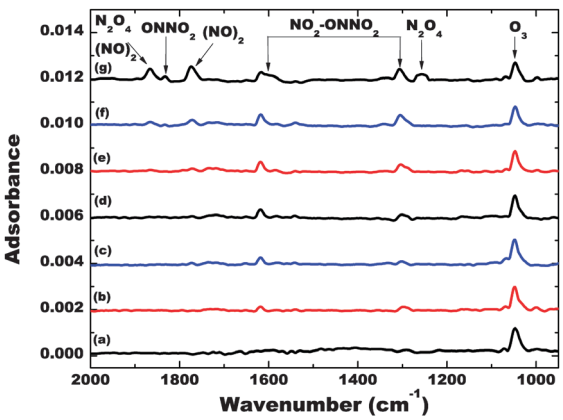

Fig. 7 Seven RAIR spectra after deposition at 10 K of 1.5 ML O_3 with increasing doses of NO from (a) to (g): 0, 0.2, 0.4, 0.6, 0.9, 1.8, and 3.5 ML of NO.

of layering effects, *i.e.*, for a high NO coverage, the top NO layers will not react with O_3 molecules since ozone is shielded by the underlying NO molecules. This effect is partially visible in Fig. 7, where it is possible to follow the (dis)appearance of spectral features as a function of NO coverage. The spectrum in panel (a) is obtained after deposition of 1.5 ML O_3 (1043 cm^{-1}, see Table 2). The NO coverage increases from 0.2 ML (curve b) to 3.5 ML (curve g), while the intensity of the O_3 band slowly decreases, and that of the nitrogen oxide bands (NO_2, $ONNO_2$, N_2O_4 and $(NO)_2$) increases.

In line with the spectra recorded for NO + O and NO + O_2 we assign the bands at 1874 and 1773 cm^{-1} to the NO dimer.[52] N_2O_4 is found at 1874 cm^{-1}.[53] The broad band at 1307 cm^{-1} is attributed to the ν(N–O) symmetric stretch of NO_2 (or $ONNO_2$) and the band at 1612 cm^{-1} to the ν(N–O) asymmetric stretch of NO_2 (or $ONNO_2$).[54,55] The band at 1838 cm^{-1} is due to the asymmetric stretch of $ONNO_2$.[56]

Similar experiments have been conducted on a surface of non-porous (compact) amorphous solid water ice and no evident differences – except for small band shifts – have been found.

3.4 NO + N

This reaction has been studied before,[42] and is presented here for completeness, to show the full N–O solid state chemical network.

Fig. 8 shows three RAIR spectra recorded at a gold sample held at 15 K using N_2 dissociation. In curve (a) the resulting spectrum of co-deposition of N atoms at 15 K is shown (N : N_2 = 1 : 100); curve (b) shows co-deposition of N_2 (dissociation "off") with NO molecules (N_2 : NO = 100 : 500) at 15 K, while curve (c) results from co-deposition of N atoms with NO molecules (N : N_2 : NO = 1 : 100 : 500) at 15 K.

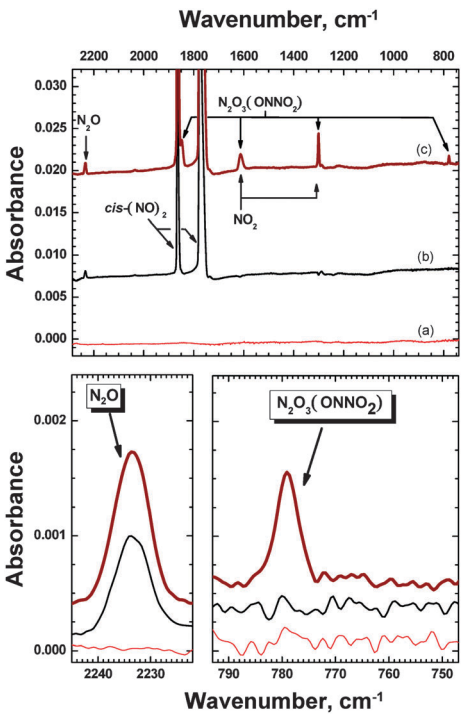

Fig. 8 In the top image three RAIR spectra are shown: (a) co-deposition of N atoms at 15 K (N : N_2 = 1 : 100); (b) co-deposition of N_2 (plasma "off") with NO molecules (N_2 : NO = 100 : 500) at 15 K; and (c) co-deposition of N atoms with NO molecules (N : N_2 : NO = 1 : 100 : 500) at 15 K. On the bottom picture regions of the spectra are magnified to indicate observed formation of dinitrogen trioxide ($ONNO_2$) on the right panel and of N_2O on the left panel.

In curve (a) we cannot identify any spectral features while curves (b) and (c) present features due to added NO, *i.e.*, the two *cis*-$(NO)_2$ bands at 1865 and 1771 cm^{-1}. In curve (c) we can also see two bands due to NO_2 and $ONNO_2$ at 1606 and 1307 cm^{-1}, respectively. Two more bands at 1836 and 774 cm^{-1} are assigned to $ONNO_2$. Furthermore, curves (b) and (c) show a band due to N_2O at 2245 cm^{-1}; the presence of N_2O is likely the result of contamination in the NO gas bottle. The presence of *cis*-$(NO)_2$ can be explained by a high NO concentration, while the NO_2 and $ONNO_2$ features arise from surface reactions, as will be discussed later.

4 Discussion

4.1 The solid surface reaction network

All experiments presented in Section 3 have in common that solid NO reacts with all the allotropes of oxygen (O, O_2 and O_3) and N atoms lead to a reduction of the NO abundance and the formation of new molecular species. The formation of these molecules – as concluded from the presented low temperature RAIR spectra – is explained by a set of partially coupled reactions. NO_2 is formed through reactions (1) to (3):

$$NO + O \rightarrow NO_2 \quad (1)$$

$$NO + O_2 \rightarrow NO_3 \xrightarrow{+NO} 2NO_2 \quad (2)$$

$$NO + O_3 \rightarrow NO_2 + O_2. \quad (3)$$

Reactions (4) to (6) result in the formation of more complex nitrogen oxides without actually involving any oxygen allotrope:

$$NO + NO \rightarrow (NO)_2 \quad (4)$$

$$NO + NO_2 \rightarrow ONNO_2 \quad (5)$$

$$NO_2 + NO_2 \rightarrow (NO_2)_2. \quad (6)$$

Two recombination reactions (7) and (8) lead to the formation of oxygen allotropes:[57,58]

$$O + O \rightarrow O_2 \quad (7)$$

$$O + O_2 \rightarrow O_3 \quad (8)$$

showing that the reactions NO + O, NO + O_2 and NO + O_3 cannot be studied independently of each other and cross-channels have to be taken into account. Moreover another reaction that allows the re-formation of NO should be considered:

$$NO_2 + O \rightarrow NO + O_2 \quad (9)$$

Actually, as shown in the Results section, in NO + O experiments almost all NO molecules are consumed suggesting that NO-consumption reactions (mainly reaction (1)) are quicker

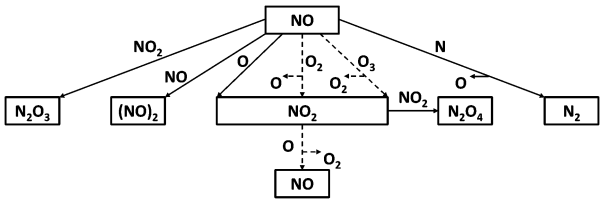

Fig. 9 Schematic representation of the reaction scheme, involving NO + $O/O_2/O_3$ reactions. Solid lines are the reactions with no barrier and dashed lines are the reactions with a small barrier.

than the NO-formation reaction (reaction (9)) (in other words $k_{NO+O} \gg k_{NO_2+O}$). For this reason we neglect reaction (9) in the present work and refer to Part II for more details.

Finally, the last reaction that we have to consider is:

$$NO + N \rightarrow N_2 + O \quad (10)$$

This reaction consumes NO and is closely linked to the other reactions. Actually by producing O-atoms, it is able to induce the formation of other molecules (the main products are NO_2 and $ONNO_2$) *via* reactions (1)–(9).

Fig. 9 shows a streamlined scheme of all possible surface reactions of NO and NO_2 molecules with O, O_2, O_3, and N. The hydrogenation of NO has been already studied in ref. 25–27. The reaction of NO with N atoms has been described in ref. 42. The channel NO + H is not shown here, as NO oxygenation is the main topic of this paper. In order to characterize the full reaction network of oxidation of NO, we start from the simplest and most independent pathway: NO + O_2. When NO arrives at the surface, it reacts either through reaction (2) or (4). In ref. 6 it was shown that the two reactions are mutually exclusive. NO_3 is the first intermediate in the reaction NO + O_2 (reaction (2)), but NO_3 is not observed in the FT-RAIR spectra. This is because NO_3 is a highly unstable molecule; if it does not react with NO to form NO_2, it will dissociate very fast yielding NO + O_2. Indeed, reactive intermediates in solid surface reaction schemes are generally hard to observe. Reaction (2) takes place during the deposition phase mainly following an Eley–Rideal (ER) mechanism. NO dimerisation together with the saturation of the ER mechanism are the limiting factors for reaction (2) to occur. Once NO_2 is formed, it can react with NO or NO_2 to form $ONNO_2$ or N_2O_4 (reactions (5) and (6)).

The reaction NO + O_3 is obviously strongly connected to reaction NO + O_2. In fact, when NO and O_3 form NO_2 and O_2 through reaction (3), solid O_2 contributes to NO_2 formation *via* reaction (2). As it is not possible to co-deposit a pure beam of O_3 – reaction (8) is far from complete – NO has been deposited on top of pre-deposited O_3. Two different phases can be distinguished. Initially when the NO coverage is low (<1 ML), O_3 adsorbed on the surface is consumed in Eley–Rideal like reactions by NO depletion from the gas phase. When NO_2 and O_2 surface densities start to increase, the NO + O_3 reaction probability decreases, and instead, reactions (2) and (5) gain in efficiency. At that stage it is unlikely that NO_2 forms following reaction (3).

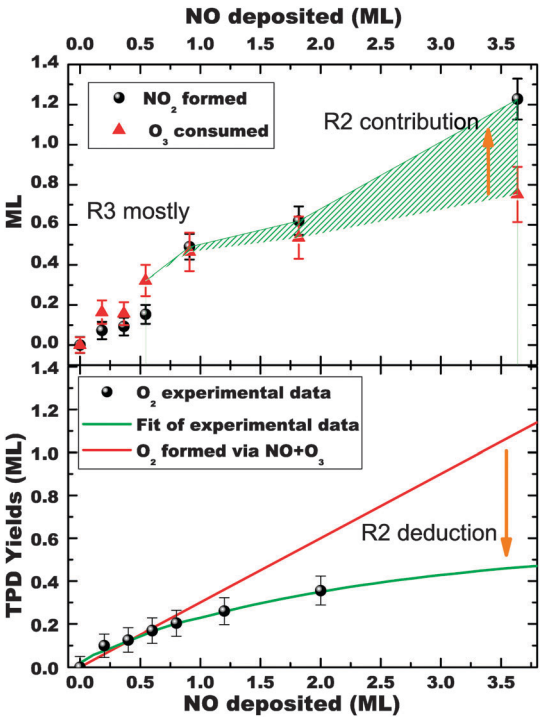

Fig. 10 Top panel: integrated area of NO_2 (black circles) and consumed O_3 (red triangles) peaks as shown in Fig. 7. Red triangles are obtained by subtracting the integrated area of O_3(NO = *x*) from O_3(NO = 0). The green pinstriped zone indicates the zone where reaction (2) starts to be efficient. Bottom panel: integrated area of O_2 TPD curves (black circles) as a function of deposited NO, and corresponding fit (green solid line); the red solid line shows the theoretical amount of O_2 formed *via* the NO + O_3 reaction.

The top panel of Fig. 10 shows the integrated area of the NO_2 and O_3 features† as shown in Fig. 7. The lower panel of Fig. 9 shows the integrated area of the TPD curves of the infrared inactive O_2 as obtained through a similar set of experiments that are not shown in the Results section. For a NO coverage lower than 1 ML, the consumption of O_3 and the formation of NO_2 behave linearly. The formation of O_2 follows a similar trend. Gradually (for NO coverages thicker than 1 ML), the formed O_2 (experimental points) starts to separate from the linear regime. This is expected as the O_2 reacts with NO through reaction (2) and O_2 cannot be formed anymore, since the NO molecules cannot react efficiently with the underlying O_3. Both effects decrease the O_2 abundance. Also O_3 is just partially consumed at this point. This is shown in Fig. 10 by the saturation of O_3. After a similar initial saturation, NO_2 concentration continues to increase (NO coverage >2 ML) through reaction (2) as shown in the pinstriped zone in Fig. 10.

Finally, the NO + O reaction is discussed. The choice of generating O atoms by dissociating N_2O or O_2 has the potential to change the reaction pathways in our experiments. When O atoms are produced through N_2O dissociation, the amount of O_2 landing on the ice is negligible and therefore only reactions (1), (4),

† The O_3 plotted in Fig. 7 is the O_3 consumed by the reactions with respect to the initial amount of O_3 (*i.e.*, O_3(NO = 0)–O_3(NO = *x*)).

and (7) are in competition. In ref. 58 it was shown that reaction (7) is barrierless or has a very small barrier. Also reaction (4) that leads to the dimerization of NO is barrierless. This is confirmed by the RAIR spectra of pure NO deposited at low temperature, where only the $(NO)_2$ features are detected (see Fig. 2). To avoid NO dimerization, NO has been deposited in a matrix of other species (*e.g.*, NO:H_2O and NO:CO, as shown in Fig. 3 and 4). In this case, the NO monomer becomes visible in the RAIR spectra, starting from polar and apolar ices, respectively. These experiments confirm the fast formation of NO_2 at low temperature also in different matrix environments.

When O-atoms are produced through O_2 dissociation, O_2 molecules can still reach the surface. This also means that O_2 can react with oxygen atoms to form O_3 (reaction (8)), specifically when the species are co-deposited. So the formation of NO_2 can occur *via* reactions (1)–(3). In the case that O + O_2 impact on already surface accreted NO molecules, reaction (3) is less probable‡ and the possible pathways are limited to reactions (1) and (2). This is the case in Fig. 1 (red line) where almost all the NO is converted into NO_2 and only a small part (about 8%) of NO molecules does not react. The incomplete conversion of NO into NO_2 is most likely not due to an activation barrier of reaction (1). It can be explained by a low penetration depth of O atoms into the NO ice, together with a small mismatch between the areas covered by the two beams (NO and O) in FORMOLISM, as well as recombination reactions O + O (O + O_2) that lead to the formation of O_2 (O_3). As O_2 (as well as newly formed O_3 molecules) is less reactive than O in reactions with NO, this can further slow down the destruction of NO and parallel formation of NO_2.

Different physical conditions have been used to constrain the reaction mechanisms. Generally, this has not resulted in pronounced dependencies as already discussed in 3.1.1 for the surface temperature and coverage. In the case of the multilayer regime experiments, the dimerization channels (reactions (4)–(6)) seem to be more efficient with respect to the sub-monolayer case, likely because of a higher density of reactants. Also the different substrates do not weight on the results strongly, mainly causing small spectral shifts as listed in Table 2.

4.2 Physical chemical processes

From a physical–chemical point of view, all our results lead to the same conclusion: NO is very reactive with N and O_x and the reaction products are nitrogen oxides. These results can be explained by having a look at the standard enthalpy of the molecules at play. Table 3 lists the standard enthalpy values (ΔH) for stable N_xO_y molecules, with x between 0 and 2 and y between 0 and 4. The values are included between 0 and 472 kJ mol^{-1}. If we do not consider the most stable (N_2 and O_2) and unstable (N and O) species, we notice that the enthalpy difference is ≈160 kJ mol^{-1}. This fact suggests that all molecules can be easily transformed into each other in the presence of O and N atoms, taking into account the activation barrier for every single case. Actually Fig. 11 is a schematic 3D representation of the N/O network, where we consider just the stable molecules. Their stability and formation enthalpies are represented vertically (the smaller the enthalpy the more stable the molecules). We have drawn the different reactions identified experimentally in this work. Presented in this way, $(NO)_2$ formation seems to be not very likely (from an energetic point of view) while NO_2, $ONNO_2$, and N_2O_4 are clearly the more stable molecules in the solid state processes involving nitrogen and oxygen.

Since the difference between enthalpies of these three molecules is very small (<73 kJ mol^{-1}) and reactions (1), (5),

‡ Actually O_3 formation is a secondary process. O + O_2 reaction is almost prevented because both O and O_2 can react with NO instead of reacting with each other to form O_3.

Table 3 List of standard enthalpy – expressed in kJ mol^{-1} and eV – for stable N_xO_y molecules

Atom/molecule	ΔH^a		
Name (molecular formula)	uma	kJ mol^{-1}	eV
Nitrogen (N)	14	472.62	4.89
Oxygen (O)	16	249.18	2.58
Molecular nitrogen (N_2)	28	0	0
Nitric oxide (NO)	30	90.29	0.94
Dioxygen (O_2)	32	0	0
Nitrous oxide (N_2O)	44	82	0.85
Nitrogen dioxide (NO_2)	46	33.1	0.34
Ozone (O_3)	48	142.67	1.48
Nitric oxide-dimer (N_2O_2 or $(NO)_2$)	60	170.33[b]	1.76[b]
Dinitrogen trioxide (N_2O_3 or $ONNO_2$)	78	82.8	0.86
Dinitrogen tetroxide N_2O_4	96	9	0.09

[a] Enthalpy values are taken from the NIST Chemistry WebBook.[59] [b] Glendening and Halpern, *J. Chem. Phys.*, 2007, **127**, 164307.[60]

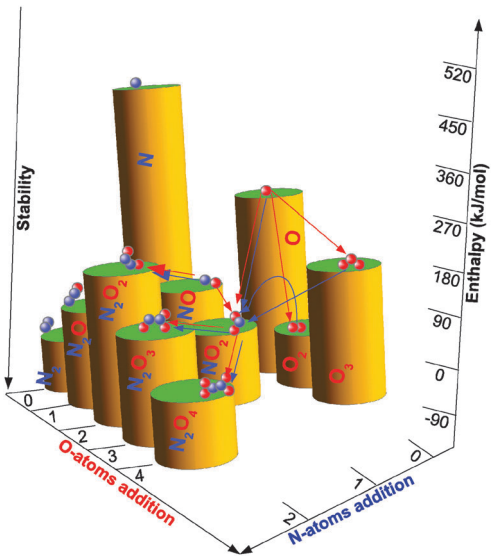

Fig. 11 Schematic 3D representation of the N/O network. The two axes in the horizontal plane represent O-atom and N-atom additions. Standard enthalpies grow along the vertical axis. The arrows represent the reaction studied in this work. In particular red and blue arrows represent O-atom and N-atom addition, respectively. The solid arrows represent barrierless reactions, while curved ones indicate reactions with an activation barrier.

(6) and (10) have no activation barrier, the ratio between N_xO_y species, in our experiments, can be explained through surface (or volume) densities of NO and O atoms (N atoms). We can consider three different cases:

(1) No O atoms (N atoms), only NO molecules present. In this case just dimers of nitric oxide, $(NO)_2$, can form. The abundances are $(NO)_2 > NO \gg NO_2 = ONNO_2 = N_2O_4 = 0$.

(2) Sub-monolayer regime (low NO and O/N densities, with O $\geq$ NO or N $\geq$ NO), with or without a water (or CO) matrix. Small amounts of NO_2 can be formed and therefore the dimerization processes (reactions (5) and (6)) are limited. $(NO)_2$ reacts with O-atoms to form NO_2. In this case $NO_2 > ONNO_2 > N_2O_4 \gg NO \approx (NO)_2 \approx 0$.

(3) Multilayer regime (O $\geq$ NO). NO_2 can be formed very efficiently, it can react with NO or another NO_2. In this case $0 \approx NO \approx (NO)_2 \ll NO_2 < ONNO_2, N_2O_4$. The $ONNO_2/N_2O_4$ ratio depends on the surrounding environment:

(a) With matrix – the presence of water or CO surrounding helps the diffusion of the lightest molecules (NO) and prevents NO_2 molecules from meeting and reacting. Actually the formation of $ONNO_2$ is more likely with respect to N_2O_4. In this case $ONNO_2 > N_2O_4$.

(b) Without matrix – newly formed NO_2 molecules can react both with NO_2 and NO. In this case $ONNO_2 \approx N_2O_4$.

Clearly from an astrochemical point of view the final products are dependent not only on their stability but also on the speed of the reaction and above all on interstellar abundances of reactants, as discussed in Part II.

5 Conclusions

In the present work the surface consumption of NO has been studied *via* solid surface reactions with $O/O_2/O_3/N$ at low temperatures and under UHV conditions. From this study we draw the following conclusions:

• Oxygenation and nitrogenation routes (NO + $O/O_2/O_3/N$) have comparable effects on NO ices. The reactions NO + O/N are barrierless, while NO + O_2/O_3 present a small barrier. Actually NO + O/N routes are the most efficient in consuming NO and, by considering interstellar abundances ($O \approx N > O_2 > O_3$), they are also the most probable surface reactions on icy dust grains. From an astrophysical point of view, the difference between observed and theoretical abundance of NO is probably due to lacking destruction (*i.e.*, consumption) routes in the astrochemical models.

• NO_2 is easily formed *via* NO + $O/O_2/O_3/N$ solid surface reactions. In its turn NO_2 is very efficient to react with NO to form $ONNO_2$ or to dimerize with other NO_2 to form N_2O_4. The non-detection of NO_2 (and of course of $ONNO_2$) in the ISM may have a clear chemical reason following an efficient destruction mechanism, such as surface NO_2 + H/O/N reactions (discussed in Part II). This can lead to abundances too low to be observable with the available sensitivity and spatial resolution of the present telescopes. Clearly, from an astrophysical point of view, due to the small abundance of NO, the solid state formation of $ONNO_2$ is less probable with respect to NO_2.

• This experimental work, together with Part II, contributes to a better understanding of H/N/O chemistry in the ISM and gives an almost complete solid state network of the formation and evolution of nitrogen oxides.

The LERMA-LAMAp team acknowledges the support of the national PCMI programme founded by CNRS. M.M. and G.F. acknowledge LASSIE, a European FP7 ITN Community's Seventh Framework Programme under Grant Agreement No. 238258. Support for S.I. from the Niels Stensen Fellowship and the Marie Curie Fellowship (FP7-PEOPLE-2011-IOF-300957) is gratefully acknowledged. The work in Leiden is supported by NOVA and NWO.

References

1 E. Jenkins, *Astrophys. J.*, 2009, **700**, 1299–1348.
2 E. A. Bergin and M. Tafalla, *Annu. Rev. Astron. Astrophys.*, 2007, **45**, 339–396.
3 K. Hiraoka and T. Sato, *Radiat. Phys. Chem.*, 2001, **60**, 389.
4 E. Matar, E. Congiu, F. Dulieu, A. Momeni and J. L. Lemaire, *Astron. Astrophys.*, 2008, **492L**, 17M.
5 T. Hama, K. Kuwahata, N. Watanabe, A. Kouchi, Y. Kimura, T. Chigai and V. Pirronello, *Astrophys. J.*, 2012, **757**, 185H.
6 M. Minissale, E. Congiu, S. Baouche, H. Chaabouni, A. Moudens, F. Dulieu, G. Manicó and V. Pirronello, *Chem. Phys. Lett.*, 2013, **565**, 52.
7 K. Hiraoka, T. Miyagoshi, T. Takayama, K. Yamamoto and Y. Kihara, *Astrophys. J.*, 1998, **498**, 710.
8 D. C. B. Whittet, *Dust in the Galactic Environment*, 2nd edn, 2003.
9 K. I. Öberg, A. C. A. Boogert, K. M. Pontoppidan, S. van den Broek, F. van Dishoeck, E. S. Bottinelli, G. A. Blake and N. J. Evans, The Molecular Universe, Proceedings of the International Astronomical Union, 2011, p. 65.
10 S. B. Charnley, S. D. Rodgers and P. Ehrenfreund, *Astron. Astrophys.*, 2001, **378**, 1024–1036.
11 R. T. Garrod, S. L. W. Weaver and E. Herbst, *Astrophys. J.*, 2008, **682**, 283–302.
12 V. Wakelam, E. Herbst, J. Le Bourlot, F. Hersant, F. Selsis and S. Guilloteau, *Astron. Astrophys.*, 2010, **517**, A21.
13 E. Herbst and E. F. van Dishoeck, *Annu. Rev. Astron. Astrophys.*, 2009, **47**, 427–480.
14 H. Linnartz, J.-B. Bossa, J. Bouwman, H. M. Cuppen, S. H. Cuylle, E. F. van Dishoeck, E. C. Fayolle, G. Fedoseev, G. W. Fuchs, S. Ioppolo, K. Isokoski, T. Lamberts, K. I. Öberg, C. Romanzin, E. Tenenbaum and J. Zhen, The Molecular Universe, Proceedings of the International Astronomical Union, 2011, p. 390.
15 S. Ioppolo, H. E. Cuppen, C. Romanzin, E. F. van Dishoeck and H. Linnartz, *Astrophys. J.*, 2008, **686**, 1474.
16 F. Dulieu, L. Amiaud, E. Congiu, J.-H. Fillion, E. Matar, A. Momeni, V. Pirronello and J. L. Lemaire, *Astron. Astrophys.*, 2010, **512**, A30.
17 D. Jing, J. He, J. Brucato, A. De Sio, L. Tozzetti and G. Vidali, *Astrophys. J.*, 2011, **741L**, 9J.

18 M. D. Ward and S. D. Price, *Astrophys. J.*, 2011, **741**, 121W.
19 Y. Oba, N. Watanabe, T. Hama, K. Kuwahata, H. Hidaka and A. A. Kouchi, *Astrophys. J.*, 2012, **749**, 67.
20 H. Chaabouni, M. Minissale, G. Manicó, E. Congiu, J. A. Noble, S. Baouche, M. Accolla, J. L. Lemaire, V. Pirronello and F. Dulieu, *J. Chem. Phys.*, 2012, **137**, 234706.
21 T. Lamberts, H. M. Cuppen, S. Ioppolo and H. Linnartz, *Phys. Chem. Chem. Phys.*, 2013, **15**, 8287L.
22 F. Dulieu, E. Congiu, J. Noble, S. Baouche, H. Chaabouni, A. Moudens, M. Minissale and S. Cazaux, *Sci. Rep.*, 2013, **3**, 1338.
23 K. Hiraoka, A. Yamashita, Y. Yachi, K. Aruga, T. Sato and H. Muto, *Astrophys. J.*, 1995, **443**, 363.
24 H. Hidaka, M. Watanabe, A. Kouchi and N. Watanabe, *Phys. Chem. Chem. Phys.*, 2011, **13**, 15798.
25 E. Congiu, H. Chaabouni, C. Laffon, P. Parent, S. Baouche and F. Dulieu, *J. Chem. Phys.*, 2012, **137**, 054713.
26 G. Fedoseev, S. Ioppolo, T. Lamberts, J. F. Zhen, H. M. Cuppen and H. Linnartz, *J. Chem. Phys.*, 2012, **137**, 054714.
27 E. Congiu, G. Fedoseev, S. Ioppolo, F. Dulieu, H. Chaabouni, S. Baouche, J. Lemaire, C. Laffon, P. Parent, T. Lamberts, H. M. Cuppen and H. Linnartz, *Astrophys. J.*, 2012, **750**, L12.
28 P. R. Joshi, E. L. Zins and L. Krim, *Mon. Not. R. Astron. Soc.*, 2012, **419**, 1713.
29 H. Listz and B. Turner, *Astrophys. J.*, 1978, **L73**, 224.
30 G. A. Blake, C. R. Masson, T. G. Phillips and E. C. Sutton, *Astrophys. J., Suppl. Ser.*, 1986, **60**, 357–374.
31 M. Gerin, Y. Viala, F. Pauzat and Y. Ellinger, *Astron. Astrophys.*, 1992, **266**, 463–478.
32 D. Halfen, A. J. Apponi and L. M. Zyrius, *Astrophys. J.*, 2001, **561**, 244.
33 M. Akyilmaz, D. R. Flower, P. Hily-Blant, G. Pineau des Forêts and C. M. Walmsley, *Astron. Astrophys.*, 2005, **462**, 221–230.
34 A. Nummelin, P. Bergman, A. Hjalmarson, P. Friberg, W. M. Irvine, T. J. Millar, M. Ohishi and S. Saito, *Astrophys. J., Suppl. Ser.*, 2000, **128**, 213–243.
35 D. J. Jansen, M. Spaans, M. R. Hogerheijde and E. F. van Dishoeck, *Astron. Astrophys.*, 1995, **303**, 541.
36 S. Martín, R. Mauersberger, J. Martín-Pintado, S. García-Burillo and C. Henkel, *Astron. Astrophys.*, 2003, **411**, L465–L468.
37 G. Pineau des Forets, E. Roueff and D. R. Flower, *Mon. Not. R. Astron. Soc.*, 1990, **244**, 668–674.
38 L. Ottaviano, M. E. Palumbo, H. Rothard and G. Strazzulla, Conference Proceedings, 2000.
39 D. Sicilia, S. Ioppolo, T. Vindigni, G. A. Baratta and M. E. Palumbo, *Astron. Astrophys.*, 2012, **453**, A155.
40 P. Boduch, A. Domaracka, D. Fulvio, T. Langlinay, X. Y. Lv, M. E. Palumbo, H. Rothard and G. Strazzulla, *Astron. Astrophys.*, 2012, **544**, A30.
41 T. Millar, P. Farquhar and K. Willacy, *Astron. Astrophys., Suppl. Ser.*, 1997, **121**, 139.
42 S. Ioppolo, G. Fedoseev, T. Lamberts, C. Romanzin and H. Linnartz, *Rev. Sci. Instrum.*, 2013, **84**, 073112.
43 K. Acharyya, G. W. Fuchs, H. J. Fraser, E. F. van Dishoeck and H. Linnartz, *Astron. Astrophys.*, 2007, **466**, 1005A.
44 C. Romanzin, S. Ioppolo, H. M. Cuppen, E. F. van Dishoeck and H. Linnartz, *J. Chem. Phys.*, 2011, **134**, 4504R.
45 L. Amiaud, J.-H. Fillion, S. Baouche, F. Dulieu, A. Momeni and J. L. Lemaire, *J. Chem. Phys.*, 2006, **124**, 094702.
46 Z. Djouadi, L. D'Hendecourt, H. Leroux, A. P. Jones, J. Borg, D. Deboffle and N. Chauvin, *Astron. Astrophys.*, 2005, **440**, 179.
47 K. Tschersich, *J. Appl. Phys.*, 1998, **845**, 4065T.
48 K. Tschersich and V. von Bonin, *J. Appl. Phys.*, 2000, **87**, 2565T.
49 K. Tschersich, J. P. Fleischhauer and H. Schuler, *J. Appl. Phys.*, 2008, **104**, 034908.
50 A. Schmidt, J. Offermann and R. Anton, *Thin Solid Films*, 1996, **281**, 105S.
51 R. Anton, T. Wiegner, W. Naumann, M. Liebmann, C. Klein and C. Bradley, *Rev. Sci. Instrum.*, 2000, **71**, 1177a.
52 W. G. Fateley, H. A. Bent and B. Crawford, *J. Chem. Phys.*, 1959, **31**, A30.
53 D. Fulvio, B. Sivaraman, G. Baratta, M. Palumbo and N. Mason, *Spectrochim. Acta*, 2009, **72**, 1007.
54 M. E. Bartram and B. E. Koel, *Surf. Sci.*, 1989, **213**, 137.
55 U. Schwalke, J. E. Parmeter and W. H. Weinberg, *J. Chem. Phys.*, 1986, **84**, 4036.
56 A. Stirling, I. Papai, J. Mink and D. Salhub, *J. Chem. Phys.*, 1994, **100**, 2910.
57 M. Minissale, E. Congiu, S. Baouche, H. Chaabouni, A. Moudens, F. Dulieu, M. Accolla, S. Cazaux, G. Manicó and V. Pirronello, *Phys. Rev. Lett.*, 2013, **111**, 053201.
58 M. Minissale, E. Congiu and F. Dulieu, *J. Chem. Phys.*, 2014, **140**, 074705.
59 NIST Chemistry WebBook, http://webbook.nist.gov/chemistry/.
60 E. D. Glendening and A. M. Halpern, *J. Chem. Phys.*, 2007, **127**, 164307.
61 L. Amiaud, F. Dulieu, J.-H. Fillion, A. Momeni and J. L. Lemaire, *J. Chem. Phys.*, 2007, **127**, 144709.